Available online at www.sciencedirect.com
ScienceDirect
Applied Catalysis B: Environmental 77 (2007) 110–116
APPLIED CATALYSIS B: ENVIRONMENTAL
www.elsevier.com/locate/apcatb

Nanoscale Pd/Fe bimetallic particles: Catalytic effects of palladium on hydrodechlorination

Hsing-Lung Lien [a,*], Wei-Xian Zhang [b]

[a] Department of Civil and Environmental Engineering, National University of Kaohsiung, 811 Kaohsiung, Taiwan
[b] Department of Civil and Environmental Engineering, Lehigh University, Bethlehem, PA 18015, USA

Received 17 October 2005; received in revised form 8 June 2007; accepted 17 July 2007
Available online 3 August 2007

Abstract

Reported herein is a study on the catalytic properties of palladium for hydrodechlorination using nanoscale zero-valent iron particles. Temperature-dependent experiments and X-ray diffraction (XRD) are conducted to characterize reactions of chlorinated ethylenes with nanoscale Fe and Pd/Fe particles. XRD results suggest bimetallic structures are created as a result of Pd(II) reduction by zero-valent iron and the degree of surface palladium loading is proportional to the initial amount of palladium applied. The optimal content of palladium in the bimetallic particles for dechlorination is in the range of 1–5% by weight. XRD analyses further suggest that oxidation of iron produces mainly iron oxides. No oxidized species of palladium (e.g., PdO) is found before or after the reactions. Activation energies of the dechlorination reactions with the nanoscale Pd/Fe and Fe particles are estimated to be 31.1 and 44.9 kJ/mol, respectively. A conceptual model for the catalytic hydrodechlorination by the nanoscale Pd/Fe particles is presented.

Keywords: TCE; Palladium; Iron; Hydrodechlorination; Nanoparticles; Groundwater remediation

1. Introduction

Zero-valent iron (ZVI) has been successfully used in the treatment of various groundwater and soil contaminants including a large variety of organic (e.g., chlorinated organic solvents, PCBs) and inorganic (e.g., arsenic, chromium) compounds [1–4]. In particular, permeable reactive barriers (PRBs) containing granular ZVI have been shown to be effective for the remediation of chlorinated organic solvents in contaminated aquifer [5,6]. For those applications, ZVI serves primarily as a potent and yet cost effective electron donor or reductant for the hydrodechlorination of chlorinated solvents.

It is generally accepted that the degradation of chlorinated organic solvents by ZVI is surface-mediated [2,7]. ZVI, with a standard reduction potential (E^o) of −0.447 V, releases electrons through the classical iron corrosion reaction:

$$Fe^0 \rightarrow Fe^{2+} + 2e^- \quad (1)$$

Metallic ZVI can form redox couples with several environmentally significant and redox-amenable electron acceptors including hydrogen ions (i.e., protons), dissolved oxygen, nitrate, sulfate, and carbonate. For example, under anaerobic environments, ZVI forms an effective redox couple with water yielding ferrous iron and hydrogen gas:

$$Fe^0_{(s)} + 2H_2O_{(l)} \rightarrow Fe^{2+}_{(aq)} + H_{2(g)} + 2OH^-_{(aq)} \quad (2)$$

The roles of these potential three electron donors, namely, ZVI, ferrous iron and hydrogen gas, in the reduction of chlorinated hydrocarbons have been previously examined [2]. In their contribution, Matheson and Tratnyek [2] proposed three possible mechanisms: (i) direct reduction at the metal surface, (ii) reduction by ferrous iron, and (iii) reduction by hydrogen with catalysis. It was suggested that ferrous iron, in concert with certain ligands, may slowly reduce the chlorinated hydrocarbons and that dissolved hydrogen gas, in the absence of a suitable catalytic surface, is insufficient for the reduction of chlorinated hydrocarbons. In the presence of granular ZVI, numerous researches (e.g., [2,7]), observed the rapid transformation of various contaminants confirming the validity of the direct surface reduction model (Fig. 1).

* Corresponding author. Tel.: +886 7591 9221; fax: +886 7591 9376.
E-mail address: lien.sam@nuk.edu.tw (H.-L. Lien).

0926-3373/$ – see front matter © 2007 Elsevier B.V. All rights reserved.
doi:10.1016/j.apcatb.2007.07.014

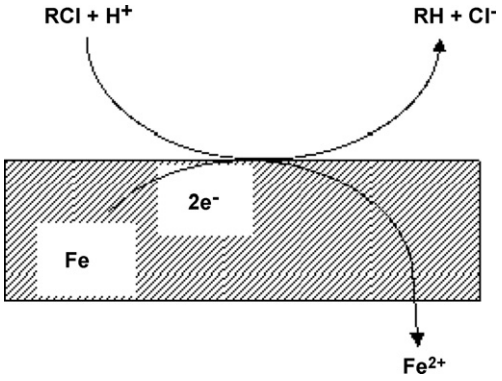

Fig. 1. Depiction of the ZVI-mediated degradation mechanism: the direct reduction model. RCl and RH represent chlorinated hydrocarbons and hydrocarbons, respectively.

Our work has focused on the research and development of nanoscale and bimetallic (e.g., Pd/Fe) ZVI particles for treatment of various contaminants including chlorinated organics (e.g., [8–10]), heavy metals [11,12] and perchlorate [13]. The synthesized nanoscale metallic particles have diameters in the range of 1–100 nm and feature 0.1–1% by weight of palladium deposited on the surface of iron. Average specific surface area of the nanoparticles is about 10–40 m^2/g, significantly greater than those of conventional granular iron powders ($\sim$1 m^2/g). Because of their small sizes, nanoscale iron particles possess a major advantage in that they can be easily delivered into subsurface via direct injection. Both laboratory and field tests have confirmed the performance of the iron nanoparticles as a remedial tool. Recent field tests have demonstrated that the nanoparticle suspension can be introduced into aquifers simply by gravity flow [14,15].

A more recent report suggested that the surface area normalized rates of carbon tetrachloride by micro and nanoscale Fe particles were by and large comparable [16]. Thus, the nano-size effect may be attributed to the increased surface area of the nanoparticles. Nonetheless, it has been observed that the products from the dechlorination of carbon tetrachloride by nanoscale Fe and Pd/Fe particles were exceedingly different [17]. The reactions of carbon tetrachloride with nanoscale Pd/Fe particles are far more complete with much higher yield of methane. Highest yield of methane (55%) and lowest production of dichloromethane (23%) was found in the use of nanoscale Pd/Fe particles. In comparison, the accumulation of dichloromethane accounted for more than 65% of initial carbon tetrachloride with less than 25% of methane production in the case of conventional microscale iron powder [17].

Similar results were also found in the reaction with chlorinated ethylenes by different types of iron. For example, reactions of bimetallic Pd/Fe nanoscale particles with tetrachloroethylene (PCE) produced ethane as the primary product (>80%) without the production of any its chlorinated intermediates (e.g., trichloroethylene, TCE). However, when PCE reacted with conventional microscale iron powder, of 38% PCE disappeared, about 13% of the original carbon was found as TCE and hydrocarbons accounted for only 15% of the PCE lost [9]. Although our earlier work have suggested that palladium plays a key role in the catalytic dechlorination and hydrogenation reactions [18], the effect of palladium has yet to be properly documented.

In this work, the catalytic properties of palladium in nanoscale ZVI particles were examined. Particle surface compositions were obtained from XRD. Temperature-dependent studies of PCE dechlorination by nanoscale Fe and Pd/Fe particles were conducted to determine activation energies of Fe and Pd/Fe nanoparticles. Considered PCE is the parent compound during the hydrodechlorination of aliphatic chlorinated ethylenes, it was selected as the model compound in the activation energy studies.

2. Experimental

2.1. Chemicals and materials

HPLC grade tetrachloroethylene (PCE, C_2Cl_4) and trichloroethylene (TCE, C_2HCl_3) were obtained from Aldrich. Sodium borohydride ($NaBH_4$, 98%) and ferric chloride ($FeCl_3{\cdot}6H_2O$, 98%) were purchased from Aldrich. Palladium acetate ($[Pd(C_2H_3O_2)_2]_3$, Pd 47.4%) was from Alfa.

2.2. Synthesis of nanoscale Pd/Fe particles

Preparation of nanoscale iron particles was achieved by adding 1:1 volume ratio of $NaBH_4$ (0.25 M) into $FeCl_3{\cdot}6H_2O$ (0.045 M) solution. Ferric iron was reduced by borohydride according to the following reaction [19]:

$$4Fe^{3+} + 3BH_4^- + 9H_2O \rightarrow 4Fe^0 + 3H_2BO_3^- + 12H^+ + 6H_2 \quad (3)$$

The suspension was mixed vigorously at room temperature (22 ± 1 °C). Palladized Fe (Pd/Fe) particles were prepared by soaking the freshly prepared nanoscale iron particles with an ethanol solution containing palladium acetate ($[Pd(C_2H_3O_2)_2]_3$). The ratio of palladium to iron was in the range of 1–50% by weight. The nanoscale Pd/Fe bimetallic particles were then washed with large volume (>1000 mL) of Milli-Q water and dried by nitrogen gas. Through sodium borohydride reduction, studies have indicated that the average diameter of iron nanoparticles is in the range of 50–100 nm and they are comprised of spherical particles assembled in chains [12]. A specific surface area of iron nanoparticles was in an average of 33.5 ± 4.2 m^2/g as measured by BET surface analyzer [11].

2.3. Batch experiments

Batch experiments were conducted in 160 mL serum bottles (150 mL nominal volume). For each batch bottle, a 20 μL methanol solution of TCE (or other targeted compounds) was spiked into a 50 mL aqueous solution to achieve the initial concentration of 120 mg/L. Nanoparticles were loaded into serum bottles at an anaerobic glove box and the metal dose was

adjusted to 5 g/L. The serum bottles were then capped with Teflon Mininert valves and mixed on a rotary shaker (30 rpm). Control tests showed the loss of carbon mass was negligible ($< \pm 10\%$) when the reactor containing no iron nanoparticles during the experimental period. In addition, no measurable difference between the use of TCE solution prepared with deionized water and that prepared with methanol in reaction with iron nanoparticles indicated the effect of minor amounts of methanol is minimum.

2.4. Temperature-dependent experiments

Temperature was controlled from 5 to 50 °C using a low temperature incubator (Model 307, Fisher Scientific). Because the headspace analysis is very sensitive to temperature, experiments were carried out under zero-headspace 160 mL serum bottles (150 mL nominal volume). PCE concentrations were analyzed by a solvent extraction method. The initial concentration of PCE was 30 mg/L and the amounts of nanoscale Fe and Pd/Fe (1 wt% Pd) particles were 1.0 and 0.25 g, respectively.

2.5. Analytic methods

2.5.1. Headspace analysis

Concentrations of chlorinated hydrocarbons were measured by a HP5890 GC-ECD equipped with a DB-624 capillary column (J&W, 30 m × 0.32 mm). Temperature conditions were programmed as follows: oven temperature at 50 °C for 5 min and then increased to 180 °C for 5 min with a rate of 20 °C/min; injection port temperature at 180 °C; and detector temperature at 300 °C.

2.5.2. Solvent extraction analysis

In the study of the temperature-dependent effect, concentrations of PCE were analyzed using a solvent extraction method as experiments were conducted in zero-headspace batch bottles. 2,2,4-Trimethylpentane (0.5 mL) was used to extract a 0.5 mL aqueous aliquot. At least 1 h extraction time was allowed prior to GC analysis. A 5 μL extractor was withdrawn for GC analysis. The analytic conditions of GC and separation column were identical as used in above described headspace analysis except a higher split ratio (up to 20). It should be pointed out that though a minor amount of nanoparticles was transferred into extraction vials during the sampling, a spike recovery study of PCE indicated that the nanoparticles in reaction with PCE is negligible during the 1 h extraction period.

2.6. XRD analysis

Solid phase analysis was conducted by an X-ray diffractometer (Philips XRD 3100 diffractometer) at 45 kV and 30 mA. The instrument used copper Kα radiation and a graphite monochromator to produce X-rays with a wavelength of 1.54060 Å. Samples were placed in a glass holder and were scanned from 20 to 60° 2θ at a rate of 2° 2θ/min. This scan range covered all major species of iron, palladium, Pd/Fe alloy, and iron oxide peaks of interest.

2.7. Kinetics analysis

The rate of transformation for PCE and TCE in a batch system was treated by a pseudo-first-order equation:

$$\frac{dC}{dt} = -k_{obs}C \quad (4)$$

where C is the concentration of chlorinated ethylenes (mg/L); k_{obs} is the measured rate constant (h^{-1}) and t is time (h). Measured first-order rate constants were calculated by the method of linear regression.

3. Results and discussion

3.1. Effect of palladium on dechlorination rates

Iron nanoparticles containing different palladium contents have been observed to exhibit drastically different reactivity toward TCE as shown in Fig. 2. The palladium content was the mass ratio of palladium to iron based on the assumption that the employed palladium was completely reduced and deposited onto the iron surface:

$$Pd^{2+} + Fe \rightarrow Pd\downarrow + Fe^{2+} \quad (5)$$

As mentioned before, ZVI and dissolved ferrous iron form a redox couple with a standard reduction potential of −0.447 V while a redox couple between zero-valent palladium and its ionic form (Pd^{2+}) has a standard reduction potential of +0.951 V. As a result, Eq. (5) is a highly thermodynamically favorable reaction (ΔE^{o} = +1.398 V). A fast conversion of Pd^{2+} to Pd^{0} was observed as the dark palladium solution quickly turned to be colorless during the course of reactions.

Kinetic data suggest that the nanoscale iron-mediated dechlorination followed a pseudo-first-order reaction where a linear regression of the test data yielded a near straight line ($R^2 > 0.95$). As shown in Fig. 2, the higher degradation rates (0.86–0.91 h^{-1}) of TCE were produced by nanoscale Pd/Fe particles with 1 and 5% palladium. In the absence of palladium, nanoscale Fe particles showed a much slower degradation rate (0.013 h^{-1}). The reactivity of nanoscale Pd/Fe particles (with 1% Pd) was greater than the unpalladized nanoscale Fe particles by a factor of about 70. Actually, substantially lower reactivity was recorded when the palladium content was increased from 10 to 20% and no reaction was found when the palladium content was increased to 50% of iron mass. In other words, the optimal performance of the bimetallic Pd/Fe particles requires a relatively small dose of palladium, a common characteristic of a catalyst.

3.2. XRD measurement

An X-ray diffraction (XRD) analysis was further conducted to determine the metal speciation on the surface of the nanoparticles. Three samples with palladium at 1, 5 and 50%

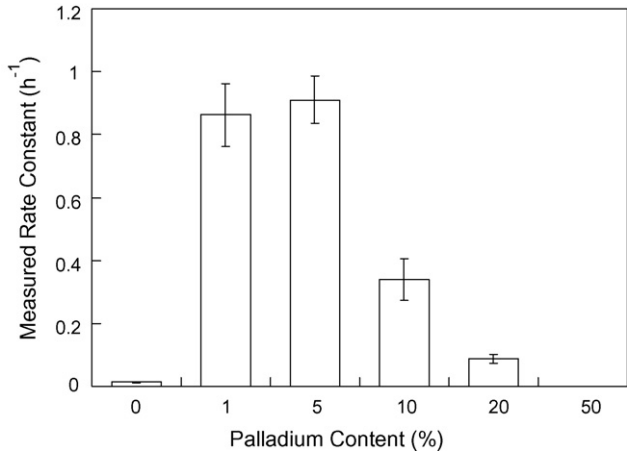

Fig. 2. Rate constant for the reduction of TCE by Pd/Fe bimetallic particles as a function of the palladium content. The initial TCE concentration was 120 mg/L and nanoparticle loading was 5 g/L.

were prepared and dried with high purity nitrogen gas. The XRD patterns of these three samples are shown in Fig. 3. The predominant features are that the samples consisted primarily of palladium metal, iron metal and iron corrosion products in various forms. The main peaks of palladium and iron corresponding to the diffraction angles (2θ) were assigned to 40.0°, and 44.9°, respectively. The observation of palladium metal on the bimetallic Pd/Fe surface is consistent with X-ray photoelectron spectra (XPS) study where the Pd 3d spectrum confirms that the palladium is present on the iron surface in the elemental state [20]. Furthermore, the grain size of Pd on the iron surface can be estimated from XRD analysis using the Scherrer's equation [21]:

$$d = \frac{0.89 \times \lambda}{B \times \cos\theta_B} \quad (6)$$

where d is the grain size (Å), λ is 1.54060 Å, B is the full width at half-maximum (FWHM) and θ_B is Bragg angle. Because the Pd peak is too small to be correctly determined in Fig. 3c, the calculation of the palladium grain size was only conducted based on Fig. 3a and b. The grain size is about 3–4 nm. It should be aware that an error for the grain size by Scherrer's equation can be up to 50%. Nevertheless, this estimation suggests that palladium deposited onto the iron surface is in the form of nanoparticles that is consistent with the conceptual model that we previously proposed [18].

In addition, various iron corrosion products including maghemite/magnetite, lepidocrocite, and hematite were identified by the XRD analysis, though several peaks still required to be further examined. These peaks were resulted accidentally from the over oxidation of fresh samples.

As shown in Fig. 3, the intensity of the palladium peak increased with increasing palladium contents. The intensity of the palladium peak and the employed amounts of palladium yielded a fairly linear relationship ($R^2 = 0.985$) (data not shown). Although the absolute quantity of the surface palladium was not determined, the result provided conclusive evidence that the palladium content on the iron surface is a function of the initial concentration of the palladium solution during the synthesis.

Experiments to compare the surface compositions of nanoscale Pd/Fe particles before and after the reaction with TCE were conducted (Fig. 4). XRD patterns of fresh particles (with 5% of palladium) were the same as in Fig. 3 while the XRD spectra of spent nanoparticles were obtained by measuring the used nanoscale Pd/Fe particles collected from the TCE degradation experiments (Fig. 2). XRD patterns indicated a relatively constant peak of palladium during the reaction. Iron consumed after 48 h generated a corresponding increase of iron oxide while little change of palladium was observed. More importantly, no oxidized species of palladium (e.g., PdO) were found before or after reactions.

For palladized iron particles, XPS analysis revealed that palladium presented in the form of elemental state on the iron surface [20]. The XRD analysis offered direct evidence to support the catalytic function(s) of the palladium in the

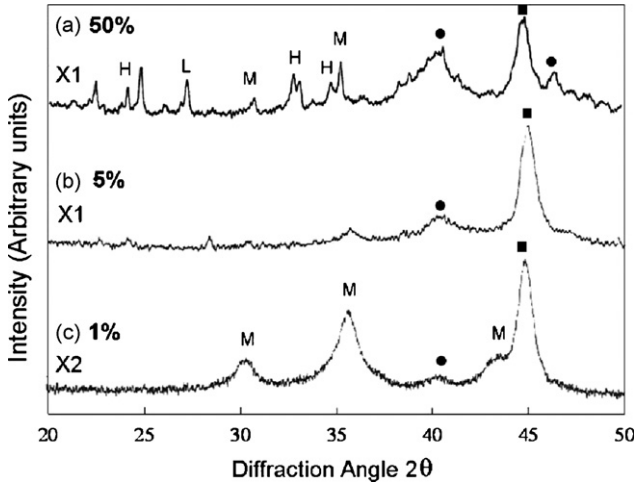

Fig. 3. XRD spectra of nanoscale Pd/Fe particles with different palladium contents. Solid square and circle represent Fe(0) and Pd(0), respectively. Iron oxides include magnetite/maghemite (Fe_3O_4/γ-Fe_2O_3) (M), hematite (α-Fe_2O_3) and lepidocrocite (γ-FeOOH) (L).

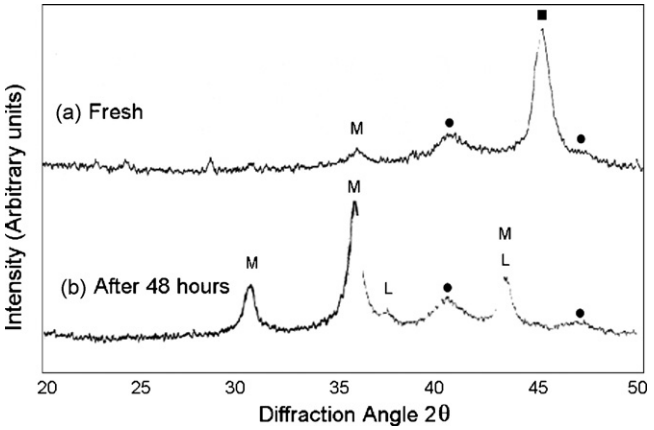

Fig. 4. Comparison of XRD spectra of nanoscale Pd/Fe particles with 5% palladium before and after reactions with TCE. Solid square and circle represent Fe(0) and Pd(0), respectively. Iron oxides include magnetite/maghemite (Fe_3O_4/γ-Fe_2O_3) (M) and lepidocrocite (γ-FeOOH) (L).

transformation of halogenated organics as the definition of a catalyst is no consumption of the catalyst itself during the reactions. Although XPS analysis was not performed in this work, it is worthy of mentioning that XPS analysis would be conducted in the further study to better confirm the speciation of palladium.

3.3. The temperature effect

Determination of reaction rates under different temperatures is often very useful in providing insights on the reaction mechanisms. Increasing temperature usually causes a significant increase in reaction rate depending on the reaction processes. A chemical reaction tends to show larger temperature dependence than does a physical process. As a result, the effect of temperature on rates of heterogeneous reactions can be used to distinguish the rate-limiting step, which may involve a chemical reaction at the surface or the diffusion of a reactant. For example, diffusion-controlled reactions in solution have relatively low activation energies (~8–21 kJ/mol), whereas the surface-controlled reactions have larger activation energies (>29 kJ/mol) [22].

Experiments on the effect of temperature were conducted to evaluate the activation energy for the dechlorination of PCE with nanoscale iron and Pd/Fe particles. An Arrhenius equation describing the relationship between rate constants and temperature was applied [22]:

$$k_{obs} = Ae^{-E_a/RT} \quad (7)$$

where k_{obs} is the measured first-order rate constant, A is a frequency factor, E_a is the activation energy, R is ideal gas constant, and T is temperature. Integrating Eq. (7) results in:

$$\ln k_{obs} = -\frac{E_a}{RT} + \ln A \quad (8)$$

Therefore, a plot of $\ln k_{obs}$ versus $1/T$ would result in a linear relationship with the slope equal to $-E_a/R$ and the intercept $\ln A$.

The activation energy for the transformation of PCE was measured in a closed batch system and temperature was varied from 5 to 50 °C. Measured rate constants were estimated by data fitting with the pseudo-first-order model as expressed in Eq. (4). Fig. 5 presents an example of pseudo-first-order regression in the PCE reaction with nanoscale Pd/Fe particles (1 wt%) at a temperature range from 5 to 50 °C. Rate constants were obtained from the slope of the straight line and are found to be reproducible in replicate tests. Values of the coefficient of determination (R^2) were greater than 0.9 in all tests. The rate constants of PCE dechlorination reactions by both nanoscale Fe and Pd/Fe particles at different temperatures are summarized in Table 1.

Fig. 6 gives the Arrhenius plots of the natural logarithm of the rate constant versus $1/T$ for the PCE dechlorination with both nanoscale Fe and Pd/Fe (1 wt%) particles. The classical Arrhenius behavior is followed in the temperature range from 5 to 50 °C. The slope of the plots was assigned as a ratio of the activation energy to the ideal gas constant. Consequently, the

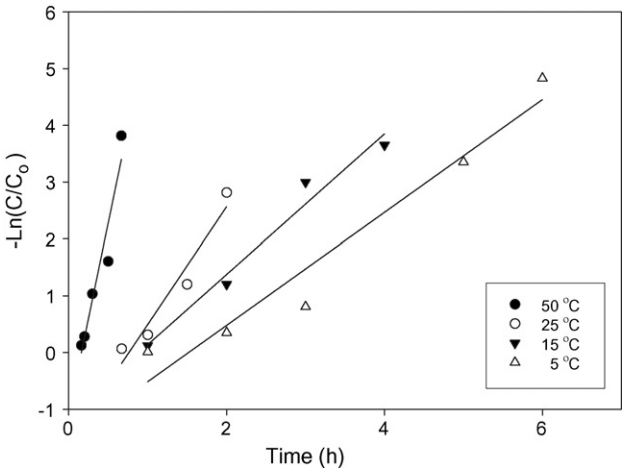

Fig. 5. A plot of $\ln(C/C_o)$ vs. time for the reduction of PCE by nanoscale Pd/Fe particles.

activation energies of dechlorination of PCE by nanoscale Pd/Fe and Fe particles are approximately 31.1 and 44.9 kJ/mol, respectively. By depositing a small amount of palladium onto the nanoscale iron surface, the activation energy is decreased by 13.8 kJ/mol. The decrease of the activation energy indicated that the dechlorination of PCE by nanoscale Pd/Fe particles is a catalytic reaction. Palladium on the iron surface serves as a catalyst.

3.4. Reaction mechanisms

In the case of surface-mediated reactions, it usually involves several steps in the overall reaction including the diffusion of a reactant to the surface, a chemical reaction on the surface, and the diffusion of a product back into the solution. The rate-limiting step, the slowest reaction step requiring the greatest activation energy, determines the overall kinetics of a reaction. In general, a typical minimum value of the activation energy for chemical-controlled reactions is ~29 kJ/mol [22]. The activation energies obtained in this study using nanoscale Pd/Fe and Fe particles are all greater than 29 kJ/mol suggesting that the surface-chemical reaction rather than diffusion is the rate-limiting step in PCE dechlorination process. Similar conclusion for the dehalogenation of TCE and carbon tetrachloride using zero-valent iron was also proposed by Su and Puls [23], and Scherer et al. [24].

Table 1
The measured rate constants of PCE dechlorination by both nanoscale Fe and Pd/Fe particles at different temperatures

Temperature (°C)	Nanoscale Pd/Fe particles		Nanoscale Fe particles	
	k_{obs} (h^{-1})	R^2	k_{obs} (h^{-1})	R^2
5	1.14	0.978	[a]	[a]
15	1.23	0.958	0.011	0.970
25	2.07	0.940	0.023	0.908
40	[a]	[a]	0.064	0.926
50	6.71	0.948	0.081	0.958

[a] No data available.

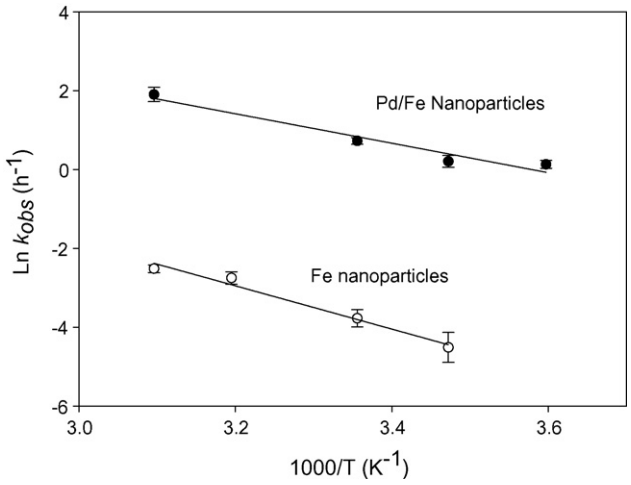

Fig. 6. The Arrhenius plot for the estimation of activation energy: dechlorination of PCE by nanoscale Fe and Fe/Pd particles.

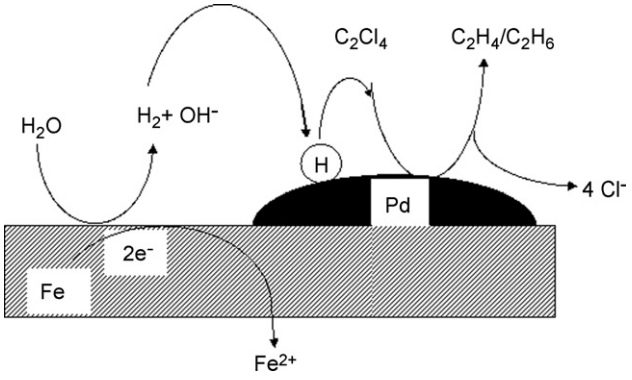

Fig. 7. A conceptual model for the hydrodechlorination of tetrachloroethylene. Atomic hydrogen is expressed as ⓗ.

Reductive dechlorination at metal surfaces involved either direct or indirect reduction or both [25,26]. Direct reduction, such as hydrogenolysis and β-elimination in the transformation of TCE by iron, may occur via formation of an organic chemisorption complex at the metal surface where metal itself serves a direct electron donor. Indirect reduction involves atomic hydrogen and no direct electron transfer from metals to reactants occurring. Atomic hydrogen is a very powerful reducing agent that reductively dechlorinates contaminants effectively [27]. Furthermore, this study and numerous investigations have shown that the catalytic hydrodechlorination by palladium usually leads to the formation of a lesser amount of chlorinated intermediates [17,28]. For example, during the course of PCE reaction with nanoscale Pd/Fe particles (1 wt%), no less-chlorinated intermediates (e.g., dichloroethylenes, and vinyl chloride) were observed. Ethane was the only product accounting for approximately 89% of the PCE lost [9]. This is likely to be attributed to the complete dissociation of carbon–chlorine bonds at the palladium surface [29,30].

In the bimetallic Pd/Fe system, because of low activation barrier for H_2 dissociation on palladium surface (2 kcal/mol or less [31]), atomic hydrogen is readily formed at the palladium surface with the low cathodic hydrogen overpotentials [26]. However, indirect reduction is much slower on metals with high hydrogen overpotentials, such as iron [26]. Taken together, a conceptual model that explains the catalytic behavior of palladium in the hydrodechlorination of chlorinated hydrocarbons is proposed (Fig. 7). The dissolution of water by ZVI leads to the hydrogen evolution (Eq. (2)) and is followed by the formation of atomic hydrogen at the palladium surface. Atomic hydrogen then degrades chlorinated hydrocarbons such as PCE through a surface-mediated process (Fig. 7). This proposed model is consistent with our previous one [18]; yet, it further explains the intrinsic function of palladium and how the proton source gets involved into the overall reaction.

4. Conclusions

Nanoscale Pd/Fe bimetallic particles have been shown an excellent performance for degradation of a wide array of contaminants in groundwater. In this study, XRD analysis indicated the bimetallic structure is formed at the surface of nanoscale Pd/Fe particles and the surface palladium coverage is proportional to the initial amount of palladium applied. The optimum content of palladium for nanoscale Pd/Fe bimetallic particles was in the range of 1–5% by weight. Both XRD analysis and the temperature-dependent study indicated that the hydrodechlorination reaction occurring in the presence of nanoscale Pd/Fe bimetallic particles is a catalytic reaction. Palladium acts as a catalyst during the reaction.

References

[1] R.W. Gillham, S.F. O'Hannesin, Ground Water 32 (1994) 958.
[2] L.J. Matheson, P.G. Tratnyek, Environ. Sci. Technol. 28 (1994) 2045.
[3] H.-L. Lien, R. Wilkin, Chemosphere 59 (2005) 377.
[4] M.J. Alowitz, M.M. Scherer, Environ. Sci. Technol. 36 (2002) 299.
[5] R.T. Wilkin, R.W. Puls, G.W. Sewell, Ground Water 41 (2003) 493.
[6] R.W. Puls, D.W. Blowes, R.W. Gillham, J. Hazard. Mater. 68 (1999) 109.
[7] E.J. Weber, Environ. Sci. Technol. 30 (1996) 716.
[8] C.B. Wang, W.-X. Zhang, Environ. Sci. Technol. 31 (1997) 2154.
[9] H.-L. Lien, W.-X. Zhang, Colloids Surf. A: Physicochem. Eng. Aspects 191 (2001) 97.
[10] H.-L. Lien, W.-X. Zhang, J. Environ. Eng. 131 (2005) 4.
[11] H.-L. Lien, Y.-S. Jhuo, L.-H. Chen, Environ. Eng. Sci. 24 (2007) 21.
[12] C. Yuan, H.-L. Lien, Water Qual. Res. J. Can. 41 (2006) 210.
[13] J. Cao, D.W. Elliott, W.-X. Zhang, J. Nanoparticle Res. 7 (2005) 499.
[14] W.-X. Zhang, J. Nanoparticle Res. 5 (2003) 323.
[15] D.W. Elliott, W.-X. Zhang, Environ. Sci. Technol. 35 (2001) 4922.
[16] J.T. Nurmi, P.G. Tratnyek, V. Sarathy, D.R. Baer, J.E. Amonette, K. Pecher, C. Wang, J.C. Linehan, D.W. Matson, R.L. Penn, M.D. Driessen, Environ. Sci. Technol. 39 (2005) 1221.
[17] H.-L. Lien, W.-X. Zhang, J. Environ. Eng. 125 (1999) 1042.
[18] W.-X. Zhang, C.-B. Wang, H.-L. Lien, Catal. Today 40 (1998) 387.
[19] G.N. Glavee, K.J. Klabunde, C.M. Sorensen, G.C. Hadjipanayis, Inorg. Chem. 34 (1995) 28.
[20] R. Muftikian, K. Nebesny, Q. Fernando, N. Korte, Environ. Sci. Technol. 30 (1996) 3593.
[21] B.D. Cullity, S.R. Stock, Elements of X-Ray Diffraction, third ed., Prentice Hall, 2001.
[22] P.L. Brezonik, Chemical Kinetics and Process Dynamics in Aquatic Systems, Lewis Publishers, 1994.
[23] C. Su, R.W. Puls, Environ. Sci. Technol. 33 (1999) 163.

[24] M.M. Scherer, J.C. Westall, M. Ziomek-Moroz, P.G. Tratnyek, Environ. Sci. Technol. 31 (1997) 2385.
[25] T. Li, J. Farrell, Environ. Sci. Technol. 34 (2000) 173.
[26] J.H. Brewster, J. Am. Chem. Soc. 76 (1954) 6361.
[27] F. Cheng, Q. Fernando, N. Korte, Environ. Sci. Technol. 31 (1997) 2443.
[28] G.V. Lowry, M. Reinhard, Environ. Sci. Technol. 33 (1999) 1905.
[29] A.H. Weiss, B.S. Gambhir, R.B. Leon, J. Catal. 22 (1971) 245.
[30] K.T. Park, K. Klier, C.B. Wang, W.-X. Zhang, J Phys. Chem. B 101 (1997) 5420.
[31] R.I. Masel, Principles of Adsorption and Reaction on Solid Surfaces, John Wiley & Sons Inc., 1996.